Anisotropic Norm-Oriented Mesh Adaptation for Compressible Inviscid Flows

Adrien Loseille, Alain Dervieux, Frédéric Alauzet

▶ **To cite this version:**

Adrien Loseille, Alain Dervieux, Frédéric Alauzet. Anisotropic Norm-Oriented Mesh Adaptation for Compressible Inviscid Flows. 53rd AIAA Aerospace Sciences Meeting, AIAA SciTech, Jan 2015, Kissimmee, Florida, United States. hal-01256131

HAL Id: hal-01256131

https://inria.hal.science/hal-01256131

Submitted on 14 Jan 2016

HAL is a multi-disciplinary open access archive for the deposit and dissemination of scientific research documents, whether they are published or not. The documents may come from teaching and research institutions in France or abroad, or from public or private research centers.

L'archive ouverte pluridisciplinaire **HAL**, est destinée au dépôt et à la diffusion de documents scientifiques de niveau recherche, publiés ou non, émanant des établissements d'enseignement et de recherche français ou étrangers, des laboratoires publics ou privés.

Anisotropic Norm-Oriented Mesh Adaptation for Compressible Inviscid Flows

Adrien Loseille *
GAMMA3 Team, INRIA Paris Rocquencourt, France

Alain Dervieux†
ECUADOR Team, INRIA Sophia-Antipolis, France

Frédéric Alauzet ‡
GAMMA3 Team, INRIA Paris Rocquencourt, France

The paper gives an unified formalism that encompasses the two most common mesh adaptation strategies: Hessian-based and goal-oriented. The first one is based on the control of the interpolation error of a solution field. The second one relies on the control of the approximation error of a scalar-output functional. Both of them have been widely used in aeronautics and derived in an anisotropic context by using a metric-based approach. If Hessian-based mesh adaptation is completely generic, it does not account for discretization error of the PDE at hand, contrary to the goal-oriented approach. The scope of this paper is to extend metric-based mesh adaptation to control a norm of the approximation error. This allows us to control simultaneously multiple functionals of interest as lift, drag, moment, without the need to solve multiple adjoint states. The procedure is based on the derivation of a corrector term that is then used as a functional for adjoint based-mesh adaptation. The estimate is derived within the continuous mesh framework, yielding naturally a fully anisotropic estimate.

Introduction

Adaptive methods in aeronautics have been used for many different purposes. The first one is generally to improve the prediction of complex phenomena (sonic-boom, contact discontinuity, blast, vortices, ...) while minimizing the CPU cost. Then, it may be used to guarantee the optimal (second) order of convergence of the numerical scheme, especially when discontinuities (shocks waves) are present in the flow field.[28] In addition, adaptivity is also concerned with the assessment of the numerical solution. We distinguish the following class of adaptive methods according to these purposes.

A first set of methods is based on the minimization of the interpolation error of one or several sensors depending on the CFD solution.[2,7,14,15,21,29,39] Given a numerical solution W_h, a solution of higher regularity $R_h(W_h)$ is recovered, so that the following interpolation error estimate[8,26] hold:

$$\|R_h(W_h) - \Pi_h R_h(W_h)\|_{L^p} \leq N^{-\frac{2}{3}} \left(\int_\Omega \det \left(|H_{R_h(W_h)}| \right)^{\frac{p}{2p+3}} \right)^{\frac{2p+3}{3p}}$$

where $H_{R_h(W_h)}$ is the Hessian of the recovered solution and N an estimate of the desired number of nodes. If anisotropic mesh prescription is naturally deduced in this context, interpolation-based methods do not take into account the features of the PDE. However, in some simplified context and assumptions (elliptic PDE, specific recovery operator), we have:

$$\|W - W_h\| \leq \frac{1}{1-\alpha} \|R_h(W_h) - \Pi_h R_h(W_h)\| \text{ with } \alpha > 1\,,$$

so that good convergence to the exact solution may be observed.[28] Indeed, if $R_h(W_h)$ is a better approximate of W in the following meaning:

$$\|W - W_h\| \ \leq \ \frac{1}{1-\alpha} \|R_h(W_h) - W_h\| \ \text{ where } \ 0 \leq \alpha < 1,$$

*Researcher, Adrien.Loseille@inria.fr
†Researcher, Alain.Dervieux@inria.fr
‡Researcher, Frederic.Alauzet@inria.fr

and if the reconstruction operator R_h has the property:

$$\Pi_h R_h(W_h) = W_h,$$

we can then bound the approximation error of the solution by the interpolation error of the reconstructed function $R_h(W_h)$:

$$\|W - W_h\| \leq \frac{1}{1-\alpha}\|R_h(W_h) - \Pi_h R_h(W_h)\|.$$

Note that from a practical point of view, $R_h(W_h)$ is never recovered, only its first and second derivatives are estimated. Standard recovery techniques include least-square, L^2-projection, green formula or the Zienkiewicz-Zhu recovery operator.

A second set of methods tends to couple adaptivity with the assessment of the numerical prediction of the flow. Goal-oriented optimal methods[20,22,27,36,40] aims at minimizing the error committed on the evaluation of a scalar functional. An usual functional is the observation of the pressure field on an observation surface γ:

$$|j(W) - j_h(W_h)| \quad \text{with} \quad j(W) = \int_\gamma \left(\frac{p - p_\infty}{p_\infty}\right)^2,$$

where W and W_h are the solution and the numerical solution of the compressible Euler equation, respectively. They do take into account the features of the PDE, through the use of an adjoint state that gives the sensitivity of W to the observed functional j. In order to solve the goal-oriented mesh optimization problem, an *a priori* analysis has been introduced[4,24] which restricts to the main asymptotic term of the local error. If a super-convergence of $|j(W) - j_h(W_h)|$ may be observed in some cases,[18,19] goal-oriented optimal methods are specialized for a given output, and in particular do not provide a convergent solution field. Indeed, the convergence of $\|W - W_h\|$ is not predicted. In addition, if the observation of multiple functionals is possible (by means of multiple adjoint states), the optimality of the mesh and the convergence properties of the approximation error may be lost.

In each case, the aforementioned adaptive strategies address specifically one goal. Consequently, it is still a challenge to find an adaptive framework that encompass all the desired requirements: anisotropic mesh prescription, asymptotic optimal order of convergence, assessment of the convergence of the numerical solution to the continuous one, control of multiple functionals of interest, ... This paper is a contribution with a first attempt to formally predict all the different requirements. Our approach is based on the design of a norm-oriented optimal method, which takes into account the PDE features, and produces an approximate solution field which does converge to the exact one. This is done by estimating a residual term $\Pi_h W - W_h$. This term naturally arise when the functional of interest is the norm $\|\Pi_h W - W_h\|_{L^2}$. The estimate is then used as a functional with the standard goal-oriented approach. To do so, we derive some correctors that estimate the implicit error. We also discuss the two standard strategies with *a priori* and *a posteriori* estimates. Contrary to the goal-oriented mesh adaptation, the functional may be now any function of approximation error. Consequently, we can observed functional of interest that is the difference between the exact and the numerical solutions. In addition, multiple functional of interest can be observed simultaneously. For instance, the norm-functional can be:

$$(\text{drag}(W) - \text{drag}(W_h))^2 + (\text{lift}(W) - \text{lift}(W_h))^2.$$

By linearizing the right-hand side (RHS), we see that the estimate (corrector) for the norm-functional depends only of $\Pi_h W - W_h$ and produces only one RHS for the goal-oriented estimation.

The paper is organized as follows. Section I briefly recalls the considered PDE and the numerical discretization. In Section II, the Hessian-based multiscale and the goal-oriented error estimates are recalled, then a new norm-oriented error analysis is derived formally. The norm-oriented mesh adaptation uses correctors to estimate the approximation error, Section III proposes two approaches for the case of the compressible Euler equations within a linear and non linear setting. Finally, Section IV applies the proposed corrector and the norm-oriented adaptation to 3D CFD problems.

I. Flow solver models

I.A. Flow equations

The compressible Euler equations for mass, momentum and energy conservation reads (with no source terms):

$$\left\{\begin{array}{rcl} \dfrac{\partial \rho}{\partial t} + \nabla \cdot (\rho \mathbf{u}) & = & 0\,, \\ \dfrac{\partial (\rho \mathbf{u})}{\partial t} + \nabla \cdot (\rho \mathbf{u} \otimes \mathbf{u}) + \nabla p & = & 0, \\ \dfrac{\partial (\rho e)}{\partial t} + \nabla \cdot ((\rho e + p)\mathbf{u}) & = & 0, \end{array}\right.$$

where ρ denotes the density, $\mathbf{u}$ the velocity, e the total energy per mass and p the pressure. This system can be rewritten under vectorial form:

$$W_t + F_1(W)_x + F_2(W)_y + F_3(W)_z = 0,$$

where W is the non-dimensioned conservative variables vector:

$$W = (\rho, \rho u, \rho v, \rho w, \rho E)^T$$

$\mathbf{F}(W) = (F_1(W), F_2(W), F_3(W))$ are the convective (Euler) flux functions:

$$\begin{array}{rcl} F_1(W) & = & (\rho u,\ \rho u^2 + p,\ \rho uv,\ \rho uw,\ u(\rho E + p))^T \\ F_2(W) & = & (\rho v,\ \rho uv,\ \rho v^2 + p,\ \rho vw,\ v(\rho E + p))^T \\ F_3(W) & = & (\rho w,\ \rho uw,\ \rho vw,\ \rho w^2 + p,\ w(\rho E + p))^T. \end{array}$$

A weak formulation of this system writes for $W \in V = \left[H^1(\Omega)\right]^5$ as follows:

$$\forall \phi \in V, \quad (\Psi(W)\,,\,\phi) = \int_\Omega \nabla\phi \cdot \mathcal{F}(W)\ \mathrm{d}\Omega + \int_\Gamma \phi\, \bar{\mathcal{F}}(W).\mathbf{n}\ \mathrm{d}\Gamma\ =\ 0, \tag{1}$$

where Γ is the boundary of the computational domain Ω, $\mathbf{n}$ the outward normal to Γ and the boundary flux $\hat{\mathcal{F}}$ contains the boundary conditions.

I.B. Spatial discretization

Equation (1) is discretized by a vertex-centered upwind finite-volume formulation applied to unstructured tetrahedra meshes. The interested reader is invited to find a detailed presentation in.[2,33] To carry out the variational analysis, it is interesting to present the finite-volume formulation as a stabilization of the Galerkin approximation.

Let $\mathcal{H}$ be a mesh of Ω composed of tetrahedra. We denote by Ω_h and Γ_h the linear approximate of Ω and Γ defined by $\mathcal{H}$. Let us introduce the following approximation space:

$$V_h\ =\ \left\{\phi_h \in V \cap \mathcal{C}^0\ \middle|\ \phi_{h|K} \text{ is affine } \forall K \text{ element of } \mathcal{H}\right\}.$$

The interpolation operator of the previous section is chosen as the usual $\mathbb{P}^1$ operator:

$$\Pi_h :\ V \cap \mathcal{C}^0 \to\ V_h \ \text{ and } \ \forall\ P_i \text{ vertex of } \mathcal{H} \ \text{ we have } \ \Pi_h\varphi(\mathbf{x}_i) = \varphi(\mathbf{x}_i).$$

The weak discrete formulation writes:

$$\begin{array}{c} \forall \phi_h \in V_h,\ (\Psi_h(W_h)\,,\,\phi_h) = 0, \\ (\Psi_h(W_h)\,,\,\phi_h) = \displaystyle\int_{\Omega_h} \nabla\phi_h \cdot \mathcal{F}_h(W_h)\ \mathrm{d}\Omega_h + \int_{\Gamma_h} \phi_h \bar{\mathcal{F}}_h(W_h).\mathbf{n}\ \mathrm{d}\Gamma_h\ =\ 0 \\ \mathcal{F}_h = \Pi_h\mathcal{F}\ ;\ \bar{\mathcal{F}}_h = \Pi_h\bar{\mathcal{F}}. \end{array} \tag{2}$$

Taking as in Relation (2) the $\mathbb{P}^1$-interpolation of the fluxes $\mathcal{F}_h$ as a discretization principle produces a finite-element scheme which is identical to the central-differenced finite-volume scheme built on the so-called median dual cells. In practice, this family of Mixed-Element-Volume schemes cannot be used in a non-dissipative purely centered version.

In,[11,34] MUSCL versions are described and analyzed. For our analysis, we consider that the scheme under study is enriched with artificial stabilisation terms. We write this as follows:

$$\forall \phi_h \in V_h, \quad \int_{\Omega_h} \nabla \phi_h \cdot \mathcal{F}_h(W_h)\ \mathrm{d}\Omega_h + \int_{\Gamma_h} \phi_h \bar{\mathcal{F}}_h(W_h).\mathbf{n}\ \mathrm{d}\Gamma_h = -\int_{\Omega_h} \phi_h\, D_h(W_h)\mathrm{d}\Omega_h, \tag{3}$$

According to,[34] the diffusion term is of higher order as soon as it is applied to the interpolation of a smooth enough field W on a sufficiently regular mesh:

$$\left| \int_{\Omega_h} \phi_h\, D_h(W_h)\mathrm{d}\Omega_h \right| \ \leq\ h^3 K(W) |\phi_h|_{L^2}\ .$$

As a result, the dissipation term is neglected in the remaining analysis.

It is now useful to introduce the linearized operators $\mathcal{A}$ (resp. $\mathcal{A}_h$) expressed in terms of Jacobians of $\mathcal{F}$ and $\bar{\mathcal{F}}$ computed at W (resp. $\mathcal{F}_h$ and $\bar{\mathcal{F}}_h$ computed at W_h):

$$\begin{gathered} \forall W \in V \quad , \quad \forall \delta W \in V \quad , \quad \mathcal{A}(W)\delta W \in (V)' \ \text{ and } \ \forall \phi \in V, \\ (\mathcal{A}(W)\delta W\ ,\ \phi) = \int_\Omega \nabla \phi \cdot \frac{\partial \mathcal{F}}{\partial W}(W)(\delta W)\ \mathrm{d}\Omega + \int_\Gamma \phi \frac{\partial \bar{\mathcal{F}}(W)}{\partial W}(\delta W).\mathbf{n}\ \mathrm{d}\Gamma = \ 0 \end{gathered} \tag{4}$$

$$\begin{gathered} \forall W_h \in V_h \quad , \quad \forall \delta W_h \in V_h \quad , \quad \mathcal{A}_h(W_h)\delta W_h \in (V_h)' \ \text{ and } \ \forall \phi_h \in V_h, \\ (\mathcal{A}_h(W_h)\delta W_h\ ,\ \phi_h) = \int_{\Omega_h} \nabla \phi_h \cdot \frac{\partial \mathcal{F}_h}{\partial W}(W_h)(\delta W_h)\ \mathrm{d}\Omega_h + \int_{\Gamma_h} \phi_h \frac{\partial \bar{\mathcal{F}}_h(W_h)}{\partial W}(\delta W_h).\mathbf{n}\ \mathrm{d}\Gamma_h = \ 0\,. \end{gathered} \tag{5}$$

$\mathcal{A}$ and $\mathcal{A}_h$ are assumed to be invertible. We use in the sequel the notations $\mathcal{A}^{-1}RHS$ and $\mathcal{A}_h^{-1}RHS_h$ for the results of solving the corresponding systems with RHS and RHS_h as right-hand sides.

II. Formal error analysis within the continuous mesh framework

The norm oriented approach is based on previous developments on anisotropic (Hessian-based) and goal-oriented mesh adaptation. In these two cases, the anisotropic mesh prescription (orientations and sizes) is given in a close form. Each of them are tightly related to interpolation error: on the solution field for Hessian-based methods, and the Euler fluxes for the goal-oriented approach. We first recall formally the derivation of these estimates in the continuous mesh framework. It leads to the definition of two *kernels* (interpolation and goal oriented) providing the optimal mesh. The norm-oriented approach is a combination of these kernels along with the derivation of a solution corrector. In this section, we focus on controlling the implicit error $\Pi_h u - u_h$. Controlling the approximation error will consists in controlling the implicit error (corrector) and the interpolation error terms simultaneously as :

$$u - u_h = u - \Pi_h u\ +\ \Pi_h u - u_h.$$

Note that the implicit error can be seen as a point-wise error between the exact solution and the numerical one. Whereas, the interpolation error can be seen as geometric deviation between the continuous solution and its $\mathbb{P}^1$ representation on the mesh. Knowing the numerical scheme and the PDE at hand is then mandatory.

II.A. Continuous mesh framework formalism

We use in the sequel the continuous mesh framework to drive our analysis. In,[25] we prove that any mesh can be represented by a continuous Riemannian metric field $\mathcal{M}$. The link between continuous mesh and discrete mesh is based on the unit mesh concept.[16] Given a Riemannian metric field $\mathcal{M}$, a unit-mesh is a mesh having:

$$\begin{aligned} &\text{for all edges of } \mathbf{e} = AB, \quad \ell_{\mathcal{M}}(\mathbf{e}) = \int_0^1 \sqrt{{}^t AB \mathcal{M}((1-t)A + tB)AB}\ \mathrm{d}t\ \in\ \left[\frac{1}{\sqrt{2}}, \sqrt{2}\right], \\ &\text{for all elements } K, \quad |K|_{\mathcal{M}} \approx \frac{\sqrt{2}}{12}. \end{aligned} \tag{6}$$

From a practical point of view, generating an anisotropic unit mesh $\mathcal{H}$ with respect to $\mathcal{M}$ requires to use any anisotropic mesh generators, see[5,9,10,13,17,22,23,29,35,38] in 3D. Conversely, given a mesh $\mathcal{H}$, the following metric field is a continuous representative of $\mathcal{H}$:

$$\mathcal{M}_P = \exp\left(\frac{\sum_{P\in K}|K|\ln(\mathcal{M}_K)}{\sum_{P\in K}|K|}\right),$$

where P is a vertex of $\mathcal{H}$ and $\mathcal{M}_K$ is the unique metric of element K, and $|K|$ the volume of K. Consequently, if u_h denotes a discrete quantity computed on a given mesh, we use equivalently the notation $u_{\mathcal{M}}$, that represents the same quantities represented on any unit mesh with respect to $\mathcal{M}$. In the case of the interpolation error, there is a strict equivalence between continuous $u - \pi_{\mathcal{M}}u$ and discrete interpolation error $u - \Pi_h u$, see.[26] The parametrization of a mesh by $\mathcal{M}$ instead of h is advantageous for *a priori* analysis with anisotropic mesh. Indeed, it exists also quantities of interest as the density, anisotropic ratios, differentiation that are well defined on $\mathcal{M}$.

II.B. Hessian-based multiscale adaptation

Let us consider a mesh $\mathcal{H}$ which is unit for a metric $\mathcal{M}$, in other words, $\mathcal{M}$ is a continuous model of $\mathcal{H}$. A Hessian-based adaptation relies on the choice of a *sensor* u depending on the state variable W. According to the continuous mesh theory,[25,26] the $\mathbb{P}^1$ interpolation error $u - \Pi_h u$ can be expressed in terms of second derivatives of u, *i.e.,* the Hessian H_u of u, and of metric $\mathcal{M}$:

$$|u - \Pi_h u| \;\equiv\; |u - \pi_{\mathcal{M}}u| \;=\; \text{trace}(\mathcal{M}^{-\frac{1}{2}}|H_u|\mathcal{M}^{-\frac{1}{2}}), \tag{7}$$

where $|H_u|$ is derived from H_u by taking the absolute value of the eigenvalues. The above expression is the continuous approximation of the $\mathbb{P}^1$ interpolation error. Minimizing $\|u - \Pi_h u\|_{L^1(\Omega_h)}$ for a given number N of vertices can be recast in the continuous setting as minimizing $\|u - \pi_{\mathcal{M}}u\|_{L^1(\Omega)}$ for a complexity $\mathcal{C}(\mathcal{M}) = N$ where calculus of variation is available. The complexity $\mathcal{C}$ of $\mathcal{M}$ is the continuous counter part of the number of vertices. Solving this optimization problem provides an optimal interpolation-based metric (continuous mesh):

$$\mathcal{M}^{opt}_{L^1}(u) = \underset{\mathcal{C}(\mathcal{M})=N}{\arg\min}\ \text{trace}(\mathcal{M}^{-\frac{1}{2}}H_u\mathcal{M}^{-\frac{1}{2}})\,.$$

The expression of the optimal continuous mesh is:

$$\mathcal{M}^{opt}_{L^1}(u) \;=\; \frac{N}{\displaystyle\int_\Omega (\det|H_u|)^{\frac{1}{3}}}(\det|H_u|)^{-\frac{1}{3}}\,|H_u|\,. \tag{8}$$

The first term of the RHS is a global normalization term set to obtain a continuous mesh with complexity N and $(\det|H_u|)^{-\frac{1}{3}}$ is a local normalization taking into account the sensitivity of the L^1 norm. Note that expressing the continuous interpolation error for the optimal metric, Relation (8), shows that second-order convergence is obtained for smooth sensor.[26] The approach can be extended to non-smooth sensor and still recovers the second-order convergence.[12,28] Relation (8) defines analytically the optimal metric (or continuous mesh). In practice, computing the optimal metric is done approximatively, *i.e.* in a discrete context with a couple (mesh,solution) denoted $(\mathcal{H}, W_h)$, and iteratively through the following fixed point algorithm. The Hessian of sensor u is replaced by a numerical sensor of higher regularity $R_h(u_h)$ computed from the numerical sensor u_h using any recovery techniques.

Algorithm 1 Hessian-based multiscale adaptation

1. Compute state W_h on mesh $\mathcal{H}$
2. Compute sensor $u_h = u(W_h)$ and $R_h(u_h)$
3. Compute optimal metric $\mathcal{M}^{opt}_{L^1}(R_h(u_h))$
4. Generate a new adapted mesh $\mathcal{H}$ which is unit for metric $\mathcal{M}^{opt}_{L^1}(R_h(u_h))$
5. If not converge, goto 1.

For the remaining analysis, it is useful to introduce the *kernel* function $\mathcal{K}_{L^1}$ that gives the optimal metric for the $\mathbb{P}^1$ interpolation error in L^1 norm as a function of the Hessian of u instead of u directly:

$$\mathcal{M}^{opt}_{L^1}(u) \;=\; \mathcal{K}_{L^1}(|H_u|)\,. \tag{9}$$

Indeed, for goal-oriented and norm-oriented analysis the kernel will be applied to more complex Hessian functions.

II.C. Goal-oriented adaptation

The Hessian-based multiscale adaptation is geometric thus generic and does not take into account the PDE from which W is obtained. On the contrary, the goal-oriented analysis relies on the considered PDE. According to Relations (1) and (3), we assume that solution W and numerical solution W_h verify:

$$\int_{\Omega} \phi \,\mathrm{div}\mathcal{F}(W) \;+\; BI \;=\; 0 \quad \text{and} \quad \int_{\Omega_h} \phi_h \,\mathrm{div}\mathcal{F}_h(W_h) \;+\; BI_h \;=\; 0, \tag{10}$$

where BI and BI_h are boundary integrals, and the discrete fluxes are simply:

$$\mathcal{F}_h(\cdot) = \Pi_h \mathcal{F}(\Pi_h(\cdot)).$$

The goal-oriented analysis relies on the minimization of the error committed on a scalar output functional j. We assume j to be smooth enough such that j can be observed through its Taylor expansion:

$$j(W) \approx j(W_h) + (\frac{\partial j}{\partial W}(W), W - W_h)$$

which leads to:

$$j(W) - j(W_h) \approx (\frac{\partial j}{\partial W}(W), W - W_h) = (g_{go}, W - W_h). \tag{11}$$

We recall in short the main result of the analysis given in Loseille et al.[27] Introducing the adjoint state W^*_{go} defined by $W^*_{go} = (\mathcal{A}^{-1})^* g_{go} \equiv \mathcal{A}^{-*} g_{go}$, we have:

$$(g_{go}, W_h - W) \quad \leq \quad \int_{\Omega_h} |\nabla W^*_{go}| \, |\mathcal{F}(W) - \Pi_h \mathcal{F}(W)| \, d\Omega_h + \int_{\Gamma_h} |W^*_{go}| \, |(\bar{\mathcal{F}}(W) - \Pi_h \bar{\mathcal{F}}(W)).\mathbf{n}| \, d\Gamma_h. \tag{12}$$

If the boundary terms are neglected, it simplifies to

$$|j(W) - j(W_h)| \approx (|\nabla W^*_{go}|, |\mathcal{F}(W) - \Pi_h \mathcal{F}(W)|). \tag{13}$$

Similarly to the previous section, from the continuous mesh theory, we get:

$$(|\nabla W^*_{go}|, |\mathcal{F}(W) - \Pi_h \mathcal{F}(W)|) \equiv (|\nabla W^*_{go}|, |\mathcal{F}(W) - \pi_{\mathcal{M}} \mathcal{F}(W)|) = \mathrm{trace}(\mathcal{M}^{-1/2} \, |\nabla W^*_{go}| \cdot |H_{\mathcal{F}(W)}| \, \mathcal{M}^{-1/2}) \,,$$

where $\mathcal{M}$ is a metric field representing the current mesh. Then, minimizing the approximation error on functional j in L^1 norm is equivalent to solve the optimization problem:

$$\mathcal{M}^{opt}_{go} = \underset{\mathcal{C}(\mathcal{M})=N}{\arg\min} \; \mathrm{trace}(\mathcal{M}^{-1/2} \, |\nabla W^*_{go}| \cdot |H_{\mathcal{F}(W)}| \, \mathcal{M}^{-1/2}) \,,$$

and $|\nabla W^*_{go}| \cdot |H_{\mathcal{F}(W)}|$ is a positive combination of symmetric matrices. Similarly to the Hessian-based error analysis where the optimal metric is given by Relation (8) and the kernel definition (9), we get:

$$\mathcal{M}^{opt}_{go}(W) = \mathcal{K}_{L^1}(|\nabla W^*_{go}| \cdot |H_{\mathcal{F}(W)}|) = \mathcal{K}_{L^1}(|\nabla(\mathcal{A}^{-*} g_{go})| \cdot |H_{\mathcal{F}(W)}|). \tag{14}$$

Note that if we want to observe many output functionals, several adjoints must be evaluated. In addition, if we want to minimize the norm of the approximation error, the above analysis cannot be applied directly.

Relation (14) gives a continuous expression of the optimal continuous mesh. In a discrete context, all the continuous quantities are evaluated on the current mesh. We use iterative Algorithm 2 to converge to the optimal solution.

Algorithm 2 Goal-oriented adaptation

1. Compute state W_h on mesh $\mathcal{H}$
2. Compute adjoint state $W^*_{go,h}$ using $g_{go,h} = \dfrac{\partial j}{\partial W}(W_h)$ and $R_h(\mathcal{F}_h(W_h))$
3. Compute optimal metric $\mathcal{M}^{opt}_{go}(W_h) = \mathcal{K}_{L^1}(|\nabla W^*_{go,h}| \cdot |H_{R_h(\mathcal{F}_h(W_h))}|)$
4. Generate a new adapted mesh $\mathcal{H}$ which is unit for metric $\mathcal{M}^{opt}_{go}(W_h)$
5. If not converge, goto 1.

II.D. Norm-oriented adaptation

We are now interested in the minimization of a semi-norm such as:

$$\|L(W) - L(W_h)\|^2_{L^2(\Omega_h)}$$

where L is given vector or scalar valued operator. Linearizing L using a Taylor expansion, we have:

$$\Big(L(W) - L(W_h), L(W) - L(W_h)\Big) \approx \left(\frac{\partial L}{\partial W}(W)(W - W_h), \frac{\partial L}{\partial W}(W)(W - W_h)\right) .$$

Introducing the adjoint operator $\left(\dfrac{\partial L}{\partial W}\right)^*$, we can rewrite:

$$\Big(L(W)-L(W_h), L(W)-L(W_h)\Big) \approx \left(\left(\frac{\partial L}{\partial W}(W)\right)^* \left(\frac{\partial L}{\partial W}(W)\right)(W - W_h), (W - W_h)\right) = (g_{no}, (W - W_h)) .$$

Now, we apply the goal-oriented analysis to minimize $(g_{no}, (W - W_h))$, that leads to the optimal norm-oriented metric:

$$\mathcal{M}^{opt}_{no}(W) = \mathcal{K}_{L^1}(|\nabla(\mathcal{A}^{-*} g_{no})| \cdot |H_{\mathcal{F}(W)}|) = \mathcal{K}_{L^1}(|\nabla W^*_{no}| \cdot |H_{\mathcal{F}(W)}|) . \tag{15}$$

where $W^*_{no} = \mathcal{A}^{-*} g_{no}$. Here, the main difficulty is to evaluate g_{no}. Indeed, contrary to the goal-oriented case, g_{no} depends on the approximation error $W - W_h$ and not only on the solution W. Consequently, it is necessary to derive an estimate of $W - W_h$, this is done by the computation of a corrector, see Section III.

Now, let us give two examples. The simplest one is to consider the L^2 norm of the approximation error:

$$\|W - W_h\|^2_{L^2(\Omega_h)} .$$

In this particular case, $\dfrac{\partial L}{\partial W}(W)$ is the identity and g_{no} reduces to the corrector itself $(W - W_h)$. A second example is controlling the approximation on the pressure p in L^2 norm:

$$\|p - p_h\|^2_{L^2(\Omega_h)} ,$$

and we have $\dfrac{\partial p}{\partial W}(W) = (\gamma - 1)\left(\dfrac{\mathbf{u}^2}{2}, -u, -v, -w, 1\right)$ and

$$\left(\frac{\partial p}{\partial W}(W)\right)^* \left(\frac{\partial p}{\partial W}(W)\right) = (\gamma - 1)^2 \begin{pmatrix} \frac{\mathbf{u}^4}{4} & -u\frac{\mathbf{u}^2}{2} & -v\frac{\mathbf{u}^2}{2} & -w\frac{\mathbf{u}^2}{2} & \frac{\mathbf{u}^2}{2} \\ -u\frac{\mathbf{u}^2}{2} & u^2 & -uv & -uw & -u \\ -v\frac{\mathbf{u}^2}{2} & -uv & v^2 & -vw & -v \\ -w\frac{\mathbf{u}^2}{2} & -uw & -vw & w^2 & -w \\ \frac{\mathbf{u}^2}{2} & -u & -v & -w & 1 \end{pmatrix} .$$

Another example is to combine several scalar output functionals:

$$(\text{drag}(W) - \text{drag}(W_h))^2 + (\text{lift}(W) - \text{lift}(W_h))^2.$$

In that case, $\dfrac{\partial L}{\partial W}$ acts like a trace operator and $\left(\dfrac{\partial L}{\partial W}\right)^*$ is a lifting by zero operator, *i.e.,* it sets non-boundary values to zero.

In practice, all the continuous quantities are evaluated on the current mesh, so does the corrector. An iterative Algorithm 3 is again considered to converge to the optimal solution.

Algorithm 3 Norm-oriented adaptation

1. Compute state W_h on mesh $\mathcal{H}$
2. Compute an approximation $g_{no,h}$ of $W - W_h$
3. Compute adjoint state $W^*_{no,h}$ and $R_h(\mathcal{F}_h(W_h))$
4. Compute optimal metric $\mathcal{M}^{opt}_{no}(W_h) = \mathcal{K}_{L^1}(|\nabla W^*_{no,h}| \cdot |H_{R_h(\mathcal{F}_h(W_h))}|)$
5. Generate a new adapted mesh $\mathcal{H}$ which is unit for metric $\mathcal{M}^{opt}_{no}(W_h)$
6. If not converge, goto 1.

III. Correctors for the compressible Euler equations

III.A. Corrector in a linear setting

In order to apply the previous analysis to the set of Euler equations, we use again the Finite-Volume / Galerkin equivalence as stated in Section I.B. The numerical and continuous solutions of the Euler equations are given by Equations (10).

A POSTERIORI ESTIMATE. To build the *a posteriori* estimate, we combine these equations:

$$\int_{\Omega_h} \phi \,\mathrm{div}(\mathcal{F}(W) - \mathcal{F}(W_h)) \;+\; BI \;=\; -\int_{\Omega_h} \phi \,\mathrm{div}\mathcal{F}(W_h) + \int_{\Omega_h} \phi_h \,\mathrm{div}\mathcal{F}_h(W_h) \;+\; BI_h$$

By using a Taylor expansion of $\mathcal{F}$, we get:

$$\int \phi \,\mathrm{div}\frac{\partial \mathcal{F}}{\partial W}\delta W \;=\; -\int \phi \,\mathrm{div}\mathcal{F}(W_h) + \int \phi_h \,\mathrm{div}\mathcal{F}_h(W_h),$$

where δW is the implicit error $\delta W = \Pi_h W - W_h$ By using the Green formula, we obtain:

$$\int \phi \,\mathrm{div}\frac{\partial \mathcal{F}}{\partial W}\delta W \;=\; +\int \mathcal{F}(W_h)\nabla\phi - \int \mathcal{F}_h(W_h)\nabla\phi_h. \tag{16}$$

In practice we take $\phi_h = 0$, then we discretise. Note that BI terms remain. In contrast to the elliptic case, the RHS will not be zero when ϕ is replaced by ϕ_h. To use this estimate, we assume we can recover from W_h a smooth solution $R_h(W_h)$ enjoying the following properties

1. $R_h(W_h)$ is smooth,
2. $R_h(W_h)$ interpolates W_h in the sense that $\Pi_h R_h(W_h) = W_h$.

We can build a quadratic representation of $R_h(W_h)$ from W_h. The proposed quadratic scheme uses $\mathbb{P}^2$ Lagrange test functions in triangle K to reconstruct a quadratic representation of the solution on K. This interpolation requires the solution nodal value at triangle vertices P_0, P_1 and P_2 , and the solution at the triangle mid-edges. We denote by P_3, P_4 and P_5 the middle of edges P_1P_2, P_2P_0 and P_0P_1, respectively. We denote by $(W_i)_{i=0,2}$ the nodal value of W_h and ∇W_i the nodal gradient of W_h. The quadratic scheme is given by:

$$R_h(W_h)(P) = \sum_{i=0}^{2} \psi_i(P)\, W_h(P_i) + \sum_{i=3}^{5} \psi_i(P)\, R_h(W_h)(P_i),$$

with:

$$\begin{cases} \psi_i(P) = \beta_i(P)\,(2\,\beta_i(P) - 1) & \text{for } i = 0, ..., 2\,, \\ \psi_i(P) = 4\,\beta_{[i]}(P)\,\beta_{[i+1]}(P) & \text{for } i = 3, ..., 5\,, \end{cases}$$

where β_i is the barycentric of P w.r.t to P_i in triangle K and $[i]$ is i modulo 3. The mid-edge values $(R_h(W_h)(P_i))_{i=3,5}$ are recovered from the nodal gradients of vertices $P_0,\ P_1,\ P_2$:

$$\begin{aligned} R_h(W_h)(P_3) &= \tfrac{1}{2}(W_1 + W_2) + \tfrac{1}{4}(\nabla W_1 + \nabla W_2) \cdot P_1P_2, \\ R_h(W_h)(P_4) &= \tfrac{1}{2}(W_0 + W_2) + \tfrac{1}{4}(\nabla W_2 + \nabla W_0) \cdot P_2P_0, \\ R_h(W_h)(P_5) &= \tfrac{1}{2}(W_0 + W_1) + \tfrac{1}{4}(\nabla W_0 + \nabla W_1) \cdot P_0P_1. \end{aligned}$$

With this scheme, we have $R_h(W_h)(P_i) = W_i$ for the nodal values, and R_h is quadratic, such that properties 1 and 2 hold. Then the last term of (16) is still zero but can be used for building an interpolation error term:

$$\int \phi\, \text{div} \frac{\partial \mathcal{F}}{\partial W} \delta W \ \approx \ + \int \nabla \phi_h\, (\mathcal{F}(W_h) - \mathcal{F}_h(W_h)). \tag{17}$$

A PRIORI ESTIMATE. To get the *a priori* estimate, we combine the two states equations, where the added last term is null:

$$\int \phi_h\, \text{div}(\mathcal{F}_h(W_h) - \mathcal{F}_h(W)) \ + \ BI_h = \ - \int \phi_h \text{div} \mathcal{F}_h(W) + \int \phi_h \text{div} + BI_h \mathcal{F}(W).$$

In a similar way, by using a Taylor expansion and Green formula, we have:

$$\int \phi\, \text{div} \frac{\partial \mathcal{F}_h}{\partial W}(-\delta W) \ = \ + \int \mathcal{F}_h(W) \nabla \phi_h - \int \mathcal{F}(W) \nabla \phi_h. \tag{18}$$

To derive the corrector equation, we approximate the RHS of Relation (18) by replacing W by W_h:

$$\int \phi\, \text{div} \frac{\partial \mathcal{F}_h}{\partial W}(-\delta W) \ = \ + \int \nabla \phi_h\, (\mathcal{F}_h(W_h) - \mathcal{F}(W)). \tag{19}$$

We observe that (17) and (19) are close to each other.

Previous correctors are straightforward to implement when an adjoint solver is already integrated in the flow solver. However, they have several weaknesses:

- There is no guarantee that the corrected solution $W_h + \delta W$ will be physical
- The approximation of the discrete fluxes $\mathcal{F}_h(W_h)$ can be far the real numerical fluxes $\mathbf{\Phi_{ij}}$.

In addition, it is also very complex to apply the numerical fluxes $\mathbf{\Phi_{ij}}$ to the recovered solution $R_h(W_h)$. Indeed, as the nodal values are the same, it is necessary to take into account the gradient variation (during the extrapolation) in the different numerical flux choices. Another strategy is used non linear correctors.

III.B. Corrector in a non linear setting

Instead of solving a linear equation to find the corrector, we build an error equation that consists in adding a source term to reduce a defect. This residual is close to the second member found in Equations (17) and (19). In the *a priori* setting, the defect is the residual of numerical flux applied to the continuous solution. Indeed, optimally, we want

$$\text{div}(\mathcal{F}_h(W)) = 0, \quad \textit{(a priori)} \tag{20}$$

when W is the exact solution and $\mathcal{F}_h$ represents the numerical scheme. Consequently, the corrected solution W_c of the current discrete solution W_h is found by solving the non linear equation:

$$\text{div}(\mathcal{F}_h(W_c)) = -S_h(W),$$

where $S_h(W)$ is the source term computed from the divergence of $\mathcal{F}_h(W)$. In our approach W is replaced by the smooth recovery $R_h(W_h)$ and we use locally a finer mesh to take into account the nodal values at mid-edges. $S_h(W)$ is then approximated as:

$$S_h(W) \approx \text{div}(\mathcal{F}_{h/2}(R_h(W_h))).$$

A transfer procedure is used to accumulate $\mathcal{F}_{h/2}(R_h(W_h))$ on the coarser mesh h. In contrast with the linear approach, the only modification in the flow solver is to take into account a residual source term. The corrected solution is found (instead of the implicit error) and the corrected solution is guarantee to be physical.

In the *a posteriori* setting, the defect is the gap between the continuous PDE with respect to the numerical solution. Indeed, ideally, W_h should verify

$$\text{div}(\mathcal{F}(W_h)) = 0, \quad \textit{(a posteriori)} \tag{21}$$

meaning that the numerical solution solves exactly the continuous set of Euler equations. In this case, the (exact) source term is the divergence of $\mathcal{F}(W_h)$. The continuous fluxes $\mathcal{F}$ are approximated on locally refined grids, so that the source term becomes the divergence of $\mathcal{F}_{h/2}(W_h)$. The solution on the finer mesh is interpolation from the coarser mesh and the source term computed on $h/2$ is accumulated back from the finer to the coarser mesh.

From a practical point of view, the finer grids are never generated as we can solve local problem to compute the source terms. The flow solver is then used to inverse the error equation directly. The procedure to derive the corrected solution is then:

Algorithm 4 Corrected solution computation

1. Solve the flow problem to get the numerical solution W_h
2. Compute the source term on finer mesh $-S_h(W)$ or $S(W_h)$
3. From W_h, converge again the solution with the residual source term added

To perform mesh adaptation, then the second member of the adjoint equation is $W_c - W_h$. A standard metric-based goal-oriented metric is used. The norm of the implicit error is then controlled.

IV. Numerical experiments

In this section, we focus on the validation of the correctors. We only consider the *a posteriori* corrector based on the residual $\mathcal{F}(W_h)$. The continuous flux $\mathcal{F}$ is approximated on a locally finer mesh while the solution is considered linearly or quadratically interpolated, with operator R_h given in Section IV. Consequently, the source terms for the corrector are then (I) $\mathcal{F}_{\frac{h}{2}}(W_h)$ and (II) $\mathcal{F}_{\frac{h}{2}}(R_h W_h)$. These correctors are validated on subsonic and transonic flows. For each case, a sequence of uniform mesh of sizes h, $h/2$, $h/4$, ... is generated leading to meshes having, $N, 8\,N, 64\,N$, ... nodes. The implicit error on the corrected and uncorrected solutions are compared. We also give the predicted corrected and uncorrected lift and drag. In these examples, the source terms (I) and (II) are computed on the following finer mesh in the sequence, so that we can compare the current corrector W_c obtained on mesh h (N) with the optimal corrector $\Pi_h W_{\frac{h}{2}}$. In other words, for a mesh of size h (N), the corrected solution should be as close as possible as the solution produced on mesh $h/2$ ($8\,N$). For the flow solver, we use a second-order finite-volume scheme using HLLC approximate Riemmann solver with minmod limiter.[1,3] The final residual is set to 10^{-9} for both the initial solution and the corrected solution. The solution is converged to the steady state by mean of an implicit hybrid LU-SGS scheme.[6,31,32,37]

Note that we do not consider the *a priori* corrector as it is more delicate to use practically, especially with flows with shocks. Indeed, if a limiter is activated while computing $R_h(W_h)$, the recovered solution may equal the initial one leading to a null correction as $\mathcal{F}_h(W) \approx \mathcal{F}_h(R_h W_h) = \mathcal{F}_h(W_h) = 0$ when W_h is a converged numerical solution.

We finally perform an adaptive simulation where we compare standard anisotropic mesh adaptation with norm oriented adaptation.

SUBSONIC BUMP EXAMPLE. We consider the extruded bump geometry[a], see Figure 1 with an inflow at Mach 0.3. computed from the initial solution and the corrected flow fields on a sequence of uniform meshes composed of 17 723, 134 381, 1 044 943 and 7 682 230 vertices respectively. As the whole flow field is corrected, all functionals of interest can be corrected simultaneously. We restrict ourselves to lift and drag. For the lift, we observe that the corrected lift converges at a higher rates that the uncorrected prediction, see Figure 2 (top right). For each size of mesh, the corrected lift is 2 to 4 times smaller than the initial solution. Similar conclusions hold for the whole flow field. The implicit error $\|\Pi_h W - W_h\|$ and $\|\Pi_h W - W_c\|$ on the density field is depicted in Figure 2 (bottom left). The corrected error converges at a higher rate showing that the point-wise error on the flow flow field is always improved with these

[a] from `http://turbmodels.larc.nasa.gov/bump.html`

correctors. Using a smooth quadratic projection of W_h on the finer mesh (corrector (II)) also improves the quality of the corrected solution in comparison with to the linear-based solution (corrector (I)). This recovery locally improves the gradients of the solution that are used when evaluating the numerical fluxes $\mathcal{F}_{\frac{h}{2}}(R_h W_h)$.

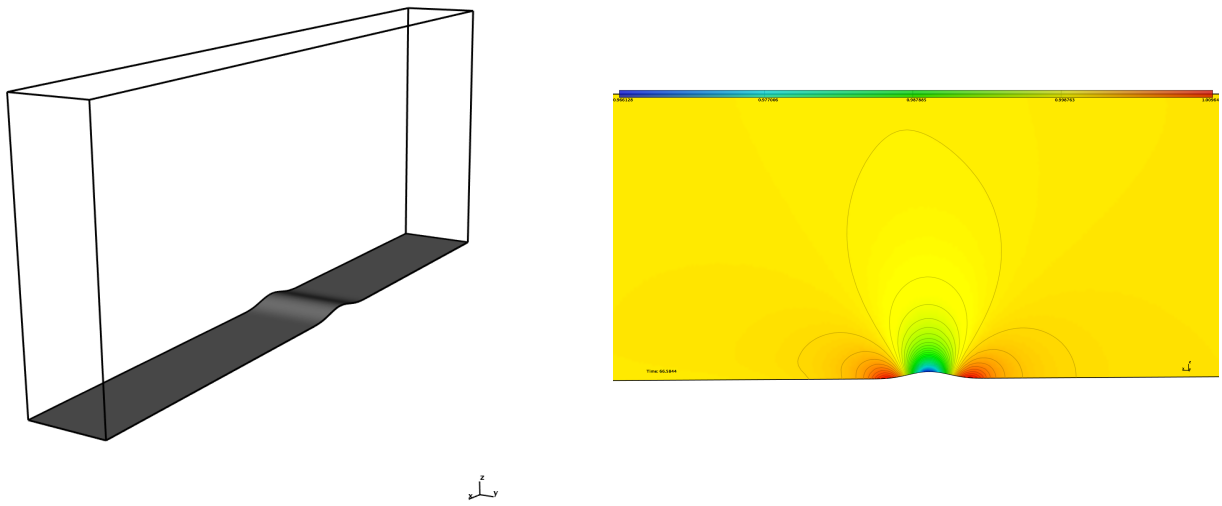

Figure 1. 3D bump geometry (left) and density flow field (right).

NACA 3D EXAMPLES. We consider the Naca0012 profile in 3D, see Figure 3 (left). From the previous test case, the geometry is no more extruded and 3D effects are present in the flow field. The sequence of meshes is composed of 1007, $4\,940$, $3\,445$, $271\,311$ and $2\,145\,390$ vertices respectively. A non uniform mesh mesh distribution is considered, the density of the mesh is increased on trailing and leading edges, see Figure 3 (right).

The subsonic flow is at Mach 0.4 with an angle of attack of 4 degrees. The comparisons of initial and corrected solutions based on (I) and (II) are reported in Figure 4. As for the bump, the corrected flow fields produce a better prediction of lift and drag. The implicit error on the density is also improved. We also observe that the corrected values for a mesh of size h are close to the predicted values of mesh $h/2$ for a substantial saving in computational cost, N instead of $8N$ in 3D. The computational cost to converge the error system is of the order of the initial system. For instance, the initial solution is converged in 250 iterations for the third mesh, and 190 iterations are needed to converge the corrected solution. The CPU times are 28mn and 34mn respectively. The overhead is due to the computation of the source term. The CPU to converge the solution on the 4th mesh is 3h50 with 308 iterations. Similar CPU times and iteration distributions are observed for the whole sequence of meshes.

We then consider a transonic flow at Mach 0.8 with an angle of attack of 3 degrees, the density iso-values are reported in Figure 5. In this case, the quadratic recovery R_h is limited in order to avoid the creation of local maxima. As for as the two previous cases, corrector (II) produces better prediction (except for the lift) than the linear based corrector even in the presence of shocks in the flow field.

ADAPTIVE EXAMPLE. We consider the geometry provided for the 1st high-lift prediction workshop (config. 1). We consider an inflow at Mach 0.2 with an angle of attack of 13 degrees. Three adaptation strategies are compared : the first one controls the interpolation error on the density, velocity and pressure in L^1 norm, the second controls the interpolation error on the Mach number while the third one is based on the norm-oriented approach and controls the norm of the approximation error $\|W - W_h\|_{L^2(\Omega_h)}$. For each case, five adaptations at fixed complexity are performed for a total of 15 adaptations with the following complexities: $[160\,000,\ 320\,000,\ 640\,000]$. This choice leads to final meshes having around 1 million vertices. The residual for the flow solver convergence is set to 10^{-9} for each case. The generation of the anisotropic meshes is done with the local remeshing strategy of.[30]

The surface meshes and the velocity iso-lines are depicted in Figure 6. Depending on the adaptation strategy, completely different flow fields are observed. The adaptation on the Mach number reveals strong shear layers at the wing tip that are not present in the norm oriented approach. On the contrary, recirculating flows are observed on the norm oriented approach while not being observed on the Mach number adaptation. This discrepancy is even more amplified in Figure 7 where the flow is observed in a cut plane along the three elements airfoil. For each case, the

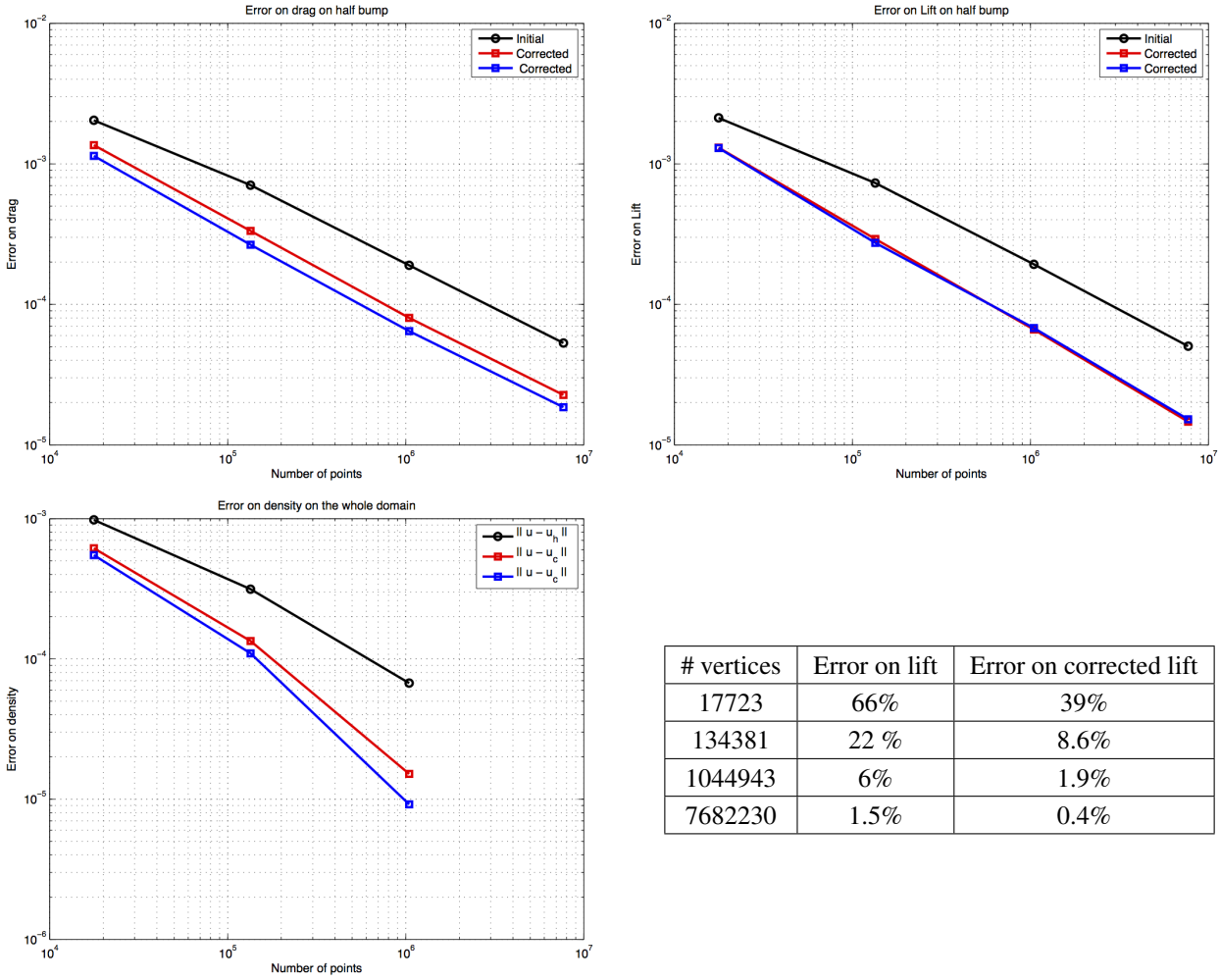

# vertices	Error on lift	Error on corrected lift
17723	66%	39%
134381	22 %	8.6%
1044943	6%	1.9%
7682230	1.5%	0.4%

Figure 2. 3D bump error on drag (top left), error on lift (top right), implicit error in $\mathbf{L}^2$ norm on the density without and with corrections (bottom right). Plain black line is the uncorrected solution while plain red lines is the corrected solution (I) based on $\mathcal{F}_{\frac{h}{2}}(W_h)$ and plain blue line is the corrected solution (II) with $\mathcal{F}_{\frac{h}{2}}(R_h W_h)$.

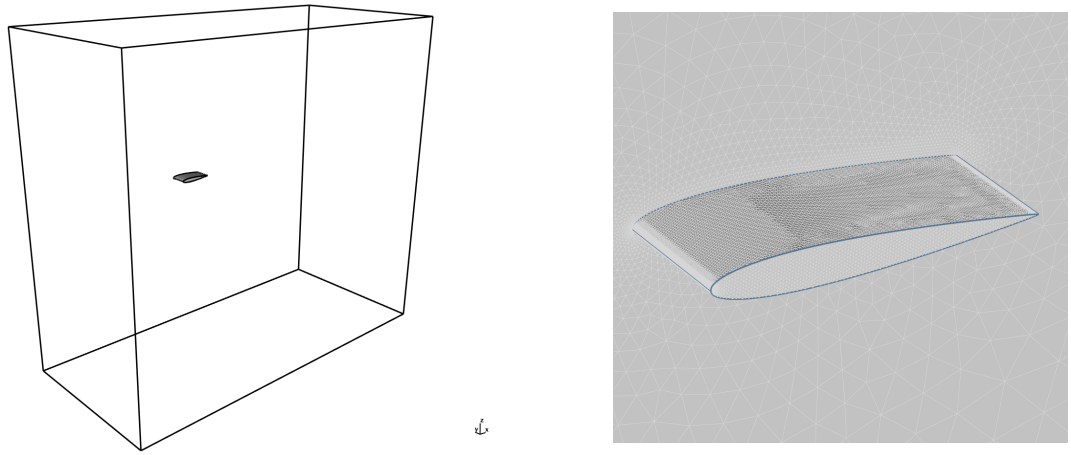

Figure 3. 3D naca geometry (left) and surface mesh (right).

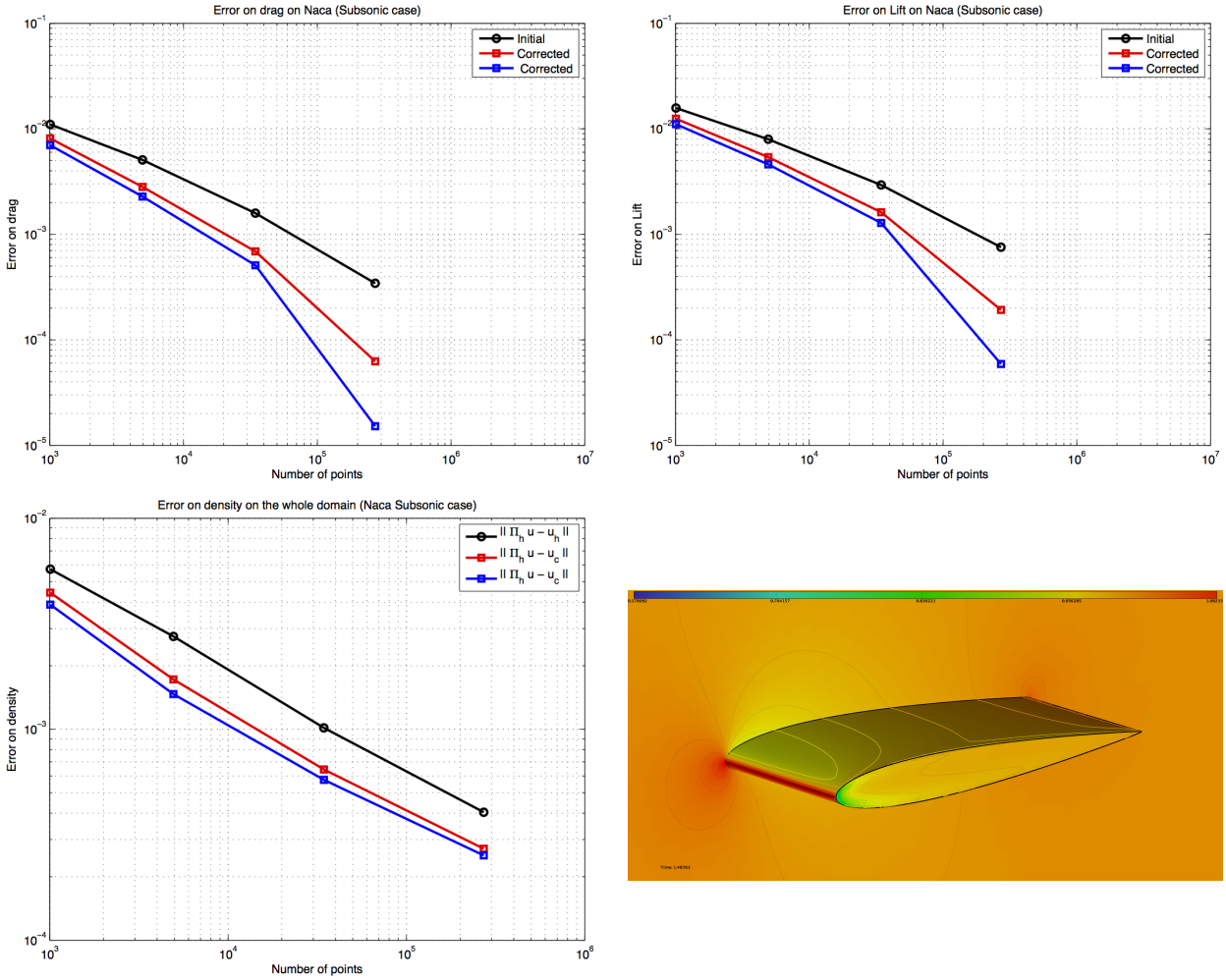

Figure 4. 3D Naca subsonic case: Error on drag (top left), error on lift (top right), implicit error in $\mathbf{L}^2$ norm on the density without and with corrections (bottom right), and density iso-values on the wing (bottom right). Plain black line is the uncorrected solution while plain red lines is the corrected solution (I) based on $\mathcal{F}_{\frac{h}{2}}(W_h)$ and plain blue line is the corrected solution (II) with $\mathcal{F}_{\frac{h}{2}}(R_h W_h)$.

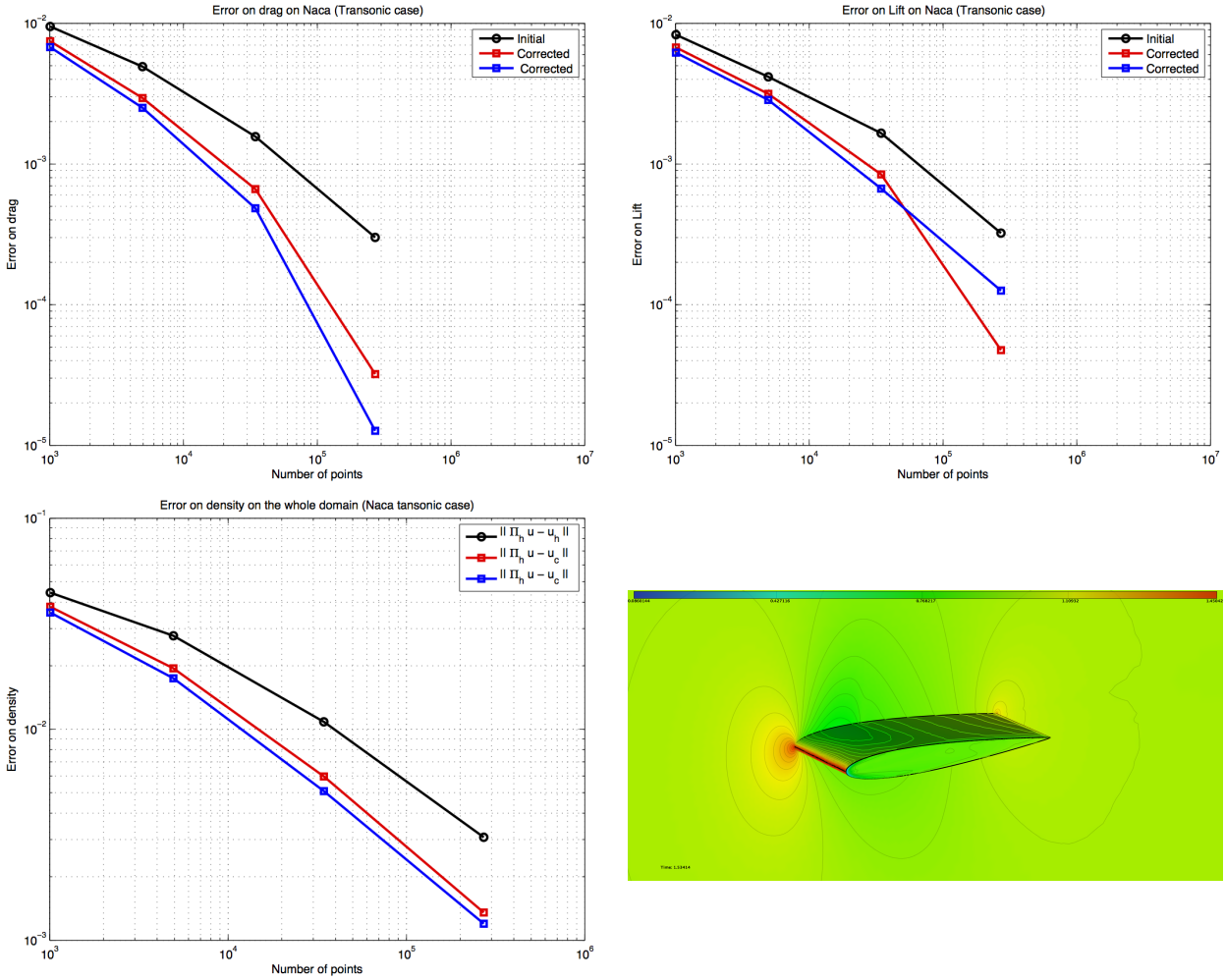

Figure 5. 3D Naca transsonic case: Error on drag (top left), error on lift (top right), implicit error in L^2 norm on the density without and with corrections (bottom right), and density iso-values on the wing (bottom right). Plain black line is the uncorrected solution while plain red lines is the corrected solution (I) based on $\mathcal{F}_{\frac{h}{2}}(W_h)$ and plain blue line is the corrected solution (II) with $\mathcal{F}_{\frac{h}{2}}(R_h W_h)$.

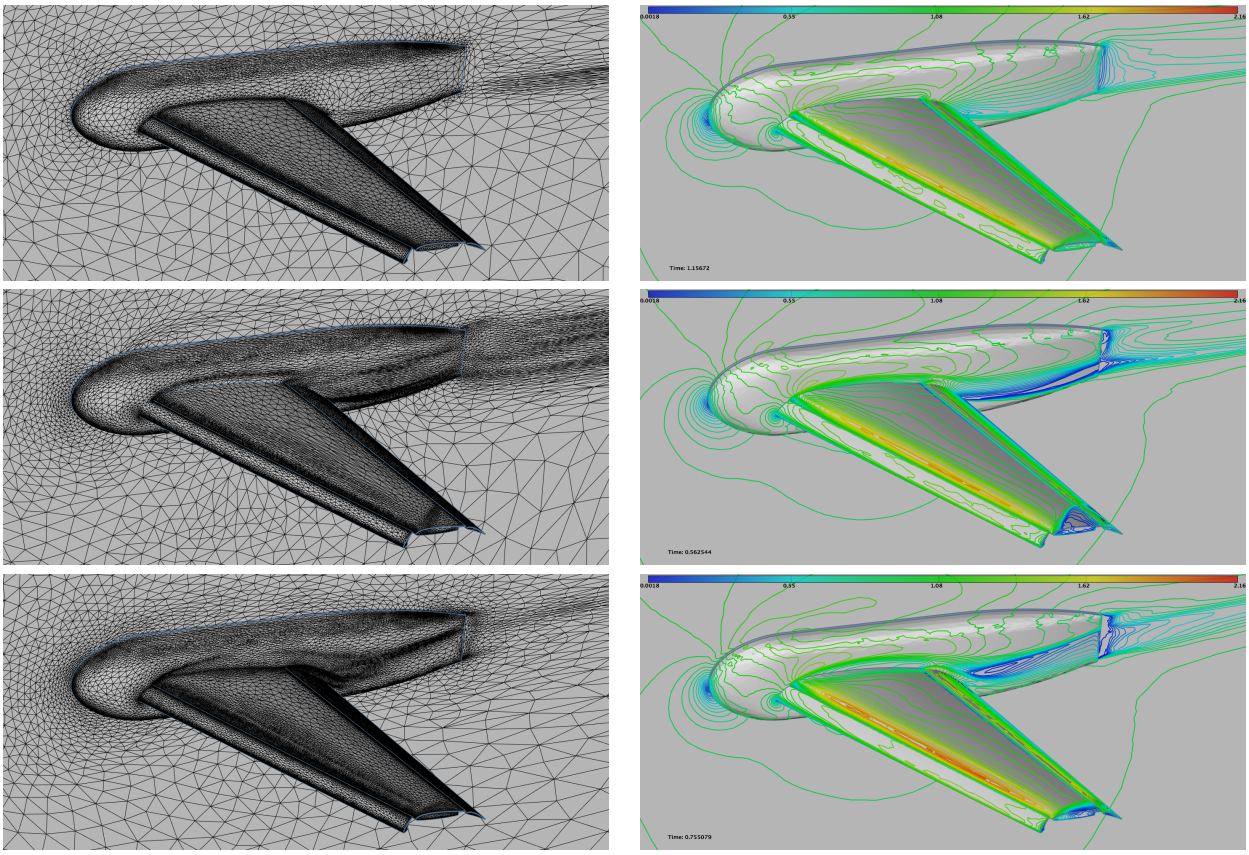

Figure 6. Surface mesh and velocity iso-values when controlling the sum of the L^1 norm of the interpolation error on the density, velocity and pressure (top), the Mach number (middle) and the norm $\|W - W_h\|_{L^2}$ with the norm oriented approach (bottom).

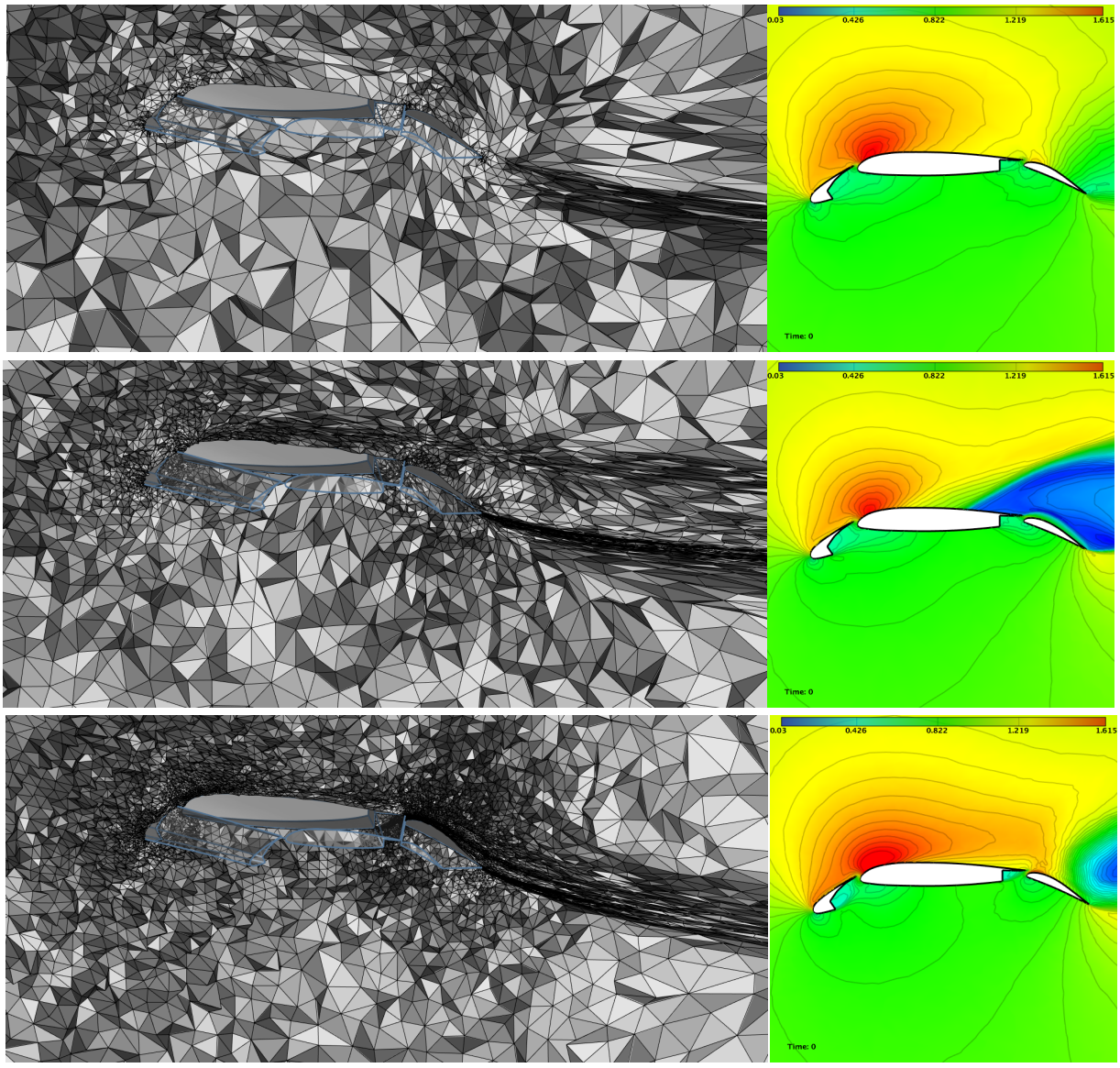

Figure 7. Cut in the volume along y-direction and velocity iso-values when controlling the sum of the L^1 norm of the interpolation error on the density, velocity and pressure (top), the Mach number (middle) and the norm $\|W - W_h\|_{L^2}$ with the norm oriented approach (bottom).

wakes have different features. Note that the accuracy near the body is not equivalent. For the L^1 norm adaptation error and norm oriented approaches, the far-field and inflow are much more refined than in the Mach number adaptation. This leads to unresolved phenomena for the final considered complexity. This example illustrates the need to control the whole flow field. Indeed, if the adaptation on the Mach number can provide a second-order convergent field, there is no guarantee on the other fields (density, pressure, velocity, ...). In addition, the adaptation with the norm-oriented approach tends to increase the refinement also at the inflow boundary condition and also at the far-field although the interpolation error (on all variables) are negligible in these areas. Consequently, it seems of main interest to control all the sources of error, especially, when the final intent is to certify a flow simulation.

Conclusion

A first step in combining into a single formalism mesh adaptation and solution correction strategies is given. It is based on *a priori* or *a posteriori* analysis of the different component of the error arising when discretizing a PDE: interpolation error, approximation error and implicit error. The interpolation is completely controlled by the derivatives of the order of the scheme. For implicit error for the Euler equations, an interpolation of the Euler fluxes is weighted by the gradient of the adjoint state with respect to the observation functional. The optimal metric is deduced from the interpolation kernel with a sum of weighted Hessian. Finally, for the norm-oriented functional, a adjoint strategy is combined with a corrector of the whole solution field is used.

We derive a simple corrector based on a computing a source term. This source term relies on the minimization of a defect of the current numerical solution. With this source term added, the flow solver is then just used as it without any more modifications required to compute the corrector: the same approximate Riemmann solver, boundary conditions and limiters are used. Contrary to standard goal-oriented approaches,[20,22,27,36,40] a corrector W_c of the whole flow field is computed. Consequently, this approach allows us to correct any set of functional of interests simultaneously. The corrected functional is simply evaluated with respect to W_c. For mesh adaptation, the corrector is used as the second member of the adjoint state, then the standard goal-oriented approach[27] is used.

Note that if a goal-oriented kernel is derived for the Navier-Stokes equations, this approach applies directly, both for the corrector and the norm-oriented adaptation.

References

[1] F. Alauzet. `Wolf` user guide. An edge-based Navier-Stokes flow solver based on the MEV numerical scheme. Internal report, INRIA, 2010.

[2] F. Alauzet and A. Loseille. High order sonic boom modeling by adaptive methods. *J. Comp. Phys.*, 229:561–593, 2010.

[3] P. Batten, M.A. Leschziner, and U.C. Goldberge. Average-state Jacobians and implicit methods for compressible viscous and turbulent flows. *J. Comp. Phys.*, 137:38–78, 1997.

[4] A. Belme, A. Dervieux, and F. Alauzet. Time accurate anisotropic goal-oriented mesh adaptation for unsteady flows. *J. Comp. Phys.*, 231:6323–6348, 2012.

[5] C.L. Bottasso. Anisotropic mesh adaption by metric-driven optimization. *Int. J. Numer. Meth. Engng*, 60:597–639, 2004.

[6] N.K. Burgess and R.S. Glasby. Advances in numerical methods for CREATE-AV analysis tools. AIAA Paper 2014-0417, National Harbor, MD, USA, Jan 2014.

[7] M. J. Castro-Díaz, F. Hecht, B. Mohammadi, and O. Pironneau. Anisotropic unstructured mesh adaptation for flow simulations. *Int. J. Numer. Meth. Fluids*, 25:475–491, 1997.

[8] L. Chen, P. Sun, and J. Xu. Optimal anisotropic meshes for minimizing interpolation errors in L^p-norm. *Math. Comp.*, 76(257):179–204, 2007.

[9] G. Compère, J.-F. Remacle, J. Jansson, and J. Hoffman. A mesh adaptation framework for dealing with large deforming meshes. *Int. J. Numer. Meth. Engng*, 82:843–867, 2010.

[10] T. Coupez. Génération de maillages et adaptation de maillage par optimisation locale. *Revue Européenne des Éléments Finis*, 9:403–423, 2000.

[11] P.-H. Cournède, B. Koobus, and A. Dervieux. Positivity statements for a Mixed-Element-Volume scheme on fixed and moving grids. *European Journal of Computational Mechanics*, 15(7-8):767–798, 2006.

[12] A. Dervieux, A. Loseille, and F. Alauzet. High-order adaptive method applied to high speed flows. In *Proceedings of WEHSFF*, 2007.

[13] C. Dobrzynski and P. J. Frey. Anisotropic delaunay mesh adaptation for unsteady simulations. In *Proc. of 17th Int. Meshing Rountable*, pages 177–194. Springer, 2008.

[14] J. Dompierre, M.G. Vallet, M. Fortin, Y. Bourgault, and W.G. Habashi. Anisotropic mesh adaptation: towards a solver and user independent CFD. In *AIAA 35th Aerospace Sciences Meeting and Exhibit*, AIAA-1997-0861, Reno, NV, USA, Jan 1997.

[15] P. J. Frey and F. Alauzet. Anisotropic mesh adaptation for CFD computations. *Comput. Methods Appl. Mech. Engrg.*, 194(48-49):5068–5082, 2005.

[16] P.J. Frey and P.-L. George. *Mesh generation. Application to finite elements*. ISTE Ltd and John Wiley & Sons, 2nd edition, 2008.

[17] P.L. George. `Gamanic3d`, adaptive anisotropic tetrahedral mesh generator. Technical Note, INRIA, 2003.

[18] M. B. Giles. On adjoint equations for error analysis and optimal grid adaptation in CFD. Technical Report NA-97/11, Oxford, 1997.

[19]M. B. Giles and N. Pierce. Improved lift and drag estimates using adjoint euler equations. *AIAA Paper* , 1999-3293, 1999.

[20]M.B. Giles and E. Suli. Adjoint methods for PDEs: a posteriori error analysis and postprocessing by duality. In *Acta Numerica*, pages 145–236. Cambridge University Press, 2002.

[21]W. Huang. Metric tensors for anisotropic mesh generation. *J. Comp. Phys.*, 204:633–665, 2005.

[22]W.T. Jones, E.J. Nielsen, and M.A. Park. Validation of 3D adjoint based error estimation and mesh adaptation for sonic boom reduction. In *44th AIAA Aerospace Sciences Meeting and Exhibit*, AIAA-2006-1150, Reno, NV, USA, Jan 2006.

[23]X. L. Li, M. S. Shephard, and M. W. Beall. 3D anisotropic mesh adaptation by mesh modification. *Comput. Methods Appl. Mech. Engrg.*, 194(48-49):4915–4950, 2005.

[24]A. Loseille. *Adaptation de maillage 3D anisotrope multi-échelles et ciblé à une fonctionnelle. Application à la prédiction haute-fidélité du bang sonique.* PhD thesis, Université Pierre et Marie Curie, Paris VI, Paris, France, 2008.

[25]A. Loseille and F. Alauzet. Continuous mesh framework. Part I: well-posed continuous interpolation error. *SIAM J. Numer. Anal.*, 49(1):38–60, 2011.

[26]A. Loseille and F. Alauzet. Continuous mesh framework. Part II: validations and applications. *SIAM J. Numer. Anal.*, 49(1):61–86, 2011.

[27]A. Loseille, A. Dervieux, and F. Alauzet. Fully anisotropic goal-oriented mesh adaptation for 3D steady Euler equations. *J. Comp. Phys.*, 229:2866–2897, 2010.

[28]A. Loseille, A. Dervieux, P.J. Frey, and F. Alauzet. Achievement of global second-order mesh convergence for discontinuous flows with adapted unstructured meshes. In *37th AIAA Fluid Dynamics Conference*, AIAA Paper 2007-4186, Miami, FL, USA, Jun 2007.

[29]A. Loseille and R. Löhner. Adaptive anisotropic simulations in aerodynamics. In *48th AIAA Aerospace Sciences Meeting*, AIAA Paper 2010-169, Orlando, FL, USA, Jan 2010.

[30]Adrien Loseille and Victorien Menier. Serial and parallel mesh modification through a unique cavity-based primitive. In Xiangmin Jiao and Jean-Christophe Weill, editors, *Proceedings of the 22nd International Meshing Roundtable*, 2013.

[31]H. Luo, J.D. Baum, and R. Löhner. A fast, matrix-free implicit method for compressible flows on unstructured grids. *J. Comp. Phys.*, 146:664–690, 1998.

[32]H. Luo, J.D. Baum, and R. Löhner. An accurate, fast, matrix-free implicit method for computing unsteady flows on unstructured grids. *Comput. & Fluids*, 30:137–159, 2001.

[33]V. Menier, A. Loseille, and F. Alauzet. CFD validation and adaptivity for viscous flow simulations. In *44th AIAA Fluid Dynamics Conference*, AIAA Paper 2014-2925, Atlanta, GA, USA, Jun 2014.

[34]K. Mer. Variational analysis of a mixed element/volume scheme with fourth-order viscosity on general triangulations. *Comput. Methods Appl. Mech. Engrg.*, 153:45–62, 1998.

[35]C. C Pain, A. P. Umpleby, C. R. E. de Oliveira, and A. J. H. Goddard. Tetrahedral mesh optimisation and adaptivity for steady-state and transient finite element calculations. *Comput. Methods Appl. Mech. Engrg.*, 190:3771–3796, 2001.

[36]P.W. Power, C.C. Pain, M.D. Piggott, F. Fang, G.J. Gorman, A.P. Umpleby, and A.J.H. Goddard. Adjoint a posteriori error measures for anisotropic mesh optimization. *Computers & Mathematics with Applications*, 52:1213–1242, 2006.

[37]D. Sharov, H. Luo, J.D. Baum, and R. Löhner. Implementation of unstructured grid GMRES+LU-SGS method on shared-memory, cache-based parallel computers. *AIAA Paper* , 2000-0927, 2000.

[38]A. Tam, D. Ait-Ali-Yahia, M. P. Robichaud, M. Moore, V. Kozel, and W. G. Habashi. Anisotropic mesh adaptation for 3D flows on structured and unstructured grids. *Comput. Methods Appl. Mech. Engrg.*, 189:1205–1230, 2000.

[39]Y.V. Vasilevski and K.N. Lipnikov. Error bounds for controllable adaptive algorithms based on a hessian recovery. *Computational Mathematics and Mathematical Physics*, 45(8):1374–1384, 2005.

[40]D. A. Venditti and D. L. Darmofal. Grid adaptation for functional outputs: application to two-dimensional inviscid flows. *J. Comp. Phys.*, 176(1):40–69, 2002.